Accurate Antenna Characterization for Wideband Synthetic Aperture Radar Processing

F-SAR Antenna Measurements in the DLR Compact Test Range

Bernd Gabler, Ralf Horn, Marc Jäger, Andreas Reigber
Microwaves and Radar Institute
Dept. of SAR-Technology
German Aerospace Center (DLR)
Oberpfaffenhofen, Germany
bernd.gabler@dlr.de

***Abstract*—The airborne F-SAR sensor, developed and operated by the DLR Microwaves and Radar Institute, provides very high resolution, fully polarimetric synthetic aperture radar (SAR) data in multiple frequency bands that are enhanced by several interferometric imaging modes. The high resolution/high bandwidth regime of operation introduces significant challenges regarding both data calibration and image formation, or focusing. This paper reviews the methods for accurate antenna characterization and the parameter extraction for SAR data processing. The antenna measurements must accurately portray interactions with the surroundings as mounted on the aircraft. The results presented concern the antenna characterization itself and illustrate how the quality of real polarimetric and interferometric SAR data is significantly improved.**

Antenna pattern characterization, Compact Test Range, SAR processing

I. INTRODUCTION

SAR sensors commonly use wideband chirp signals to illuminate targets perpendicular to the moving direction of the sensor platform. With the long transmit pulses in range and the wide antenna beams in cross-range direction, the received raw data is initially defocused. Refocusing is done in a SAR processor that uses the exact knowledge of the system transfer function and the platform motion. With the SAR principle that is based on a coherent system, the parameters must be available as complex numbers i.e. in magnitude and phase. The radar antennas are anisotropic as a function of spatial direction and demand for a three dimensional characterization in an azimuth over elevation coordinate system over frequency. The F-SAR processer that is as well developed at the Microwaves and Radar Institute allows 3D antenna pattern correction. Compensating for the antenna is a computationally intensive step in SAR processing that requires precise, three dimensional antenna measurements.

Figure 1. The F-SAR sensor installed on a Do-228-212 aircraft with the Antenna Carrier for the X, C, S and L-band antennas towards the aft

The F-SAR sensor, shown in figure 1, carries its antennas in a specially designed carrier on the right side of the aircraft cabin. Signals transmitted and received by the antennas interact with the structure of the antenna carrier to some degree depending on the frequency band and antenna position. The antenna characterization must faithfully reproduce these interactions in order to accurately describe effects encountered in practice.

II. F-SAR ANTENNA PATTERN CHARACTERISATION

Reliable radiation pattern simulation of imaging radar antennas for airborne platforms still exceeds the capabilities of today's development tools. Especially with arrangements of several elevation beam steering antennas for polarimetric SAR interferometry, the ambient aircraft cabin shows significant influence on the amplitude and phase characteristics of each individual radiation pattern.

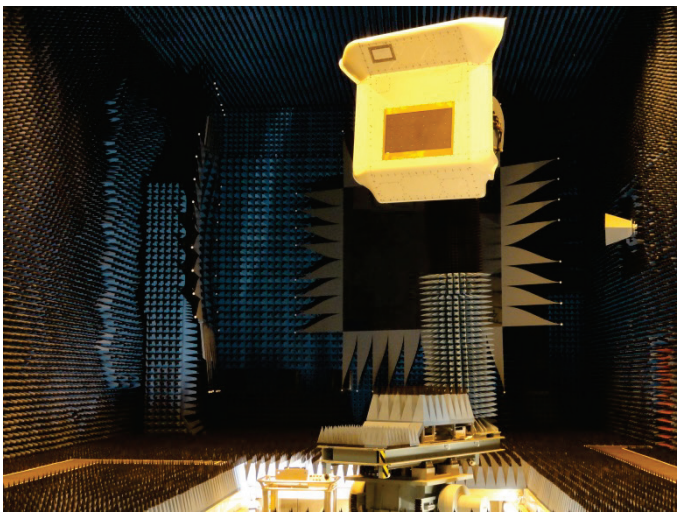

Figure 2. F-SAR Antenna Carrier in the Compact Test Range

As illustrated in figure 2, the complete F-SAR antenna carrier structure is installed in the DLR Compact Test Range to determine the antenna parameters in a complete hemisphere. Installed on a 6-axis positioner that is capable to carry AUTs with up to 300 kg, 3D theta-phi antenna patters are obtained in a roll over azimuth acquisition.

A. *Measurement procedure*

Antennas at different offset positions to the rotational center of the measurement axis and with their individual propagation delay with respect to the system phase reference can be characterized precisely in both, magnitude and phase, when signal theory parameters are carefully taken into account. Nyquist's theorem for the maximum increment Δ_{max} has to be fulfilled for the scan (azimuth) and for the step (roll) axis of the AUT positioner:

$$\Delta_{max} = {}^{1}/_{2}\,\mathrm{atan}\,\frac{c}{(R+r)f_{max}},$$

where Δ_{max} denotes the maximum angular increment of the positioner, c is the speed of light, R is the distance from the rotational center to antenna center, r is the radius of the antenna and f_{max} refers to the maximum frequency ([2], [3]).

Capturing a full-polarimetric hemisphere of a typical airborne X-Band SAR antenna with the two simultaneous measurement channels in the Compact Test Range, covers only one hour for the bare antenna. The measurement time extends to 36 hours for the same antenna on the carrier structure due to the smaller increments on both, the scan and the step axis. Motion parameters of the positioner and the measurement time of the analyzer are monitored for each individual sweep and provided to the processing chain of the antenna data. With increasing acquisition time, these corrections are essential for the phase information of the time consuming higher radar band measurements.

A large sweep bandwidth of the network analyzer signals allows an adequate downrange resolution that facilitates time domain post-processing of the acquired antenna data. Positioner velocity shall allow a high number of frequency increments within the sweep time of the signal analyzer to avoid unwanted range aliasing effects. With this method, the investigated radiating surface is enlarged from the bare antenna to the complete antenna carrier structure. The electromagnetic vectors of all parasitic scatters are superimposed with that of the radiating antenna element. Measurements now include multi-pass effects on the structure and scattering on edges that influence the antenna patterns in amplitude and phase, see figures 3 and 4, with the spherical contour plots of the X-band antenna measurements in a elevation over azimuth coordinate system

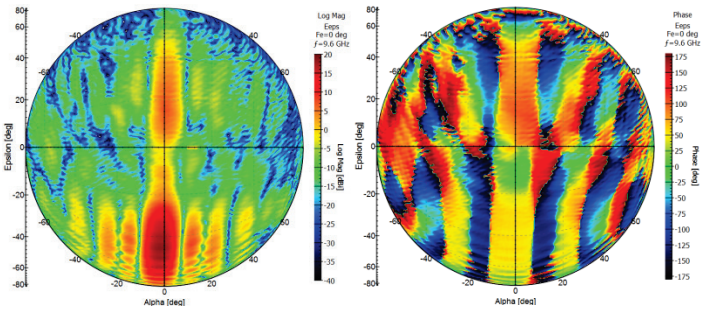

Figure 3. F-SAR X-band antenna on the top plate of the antenna carrier, left side: VV magnitude plots, right side: corrected phase plots

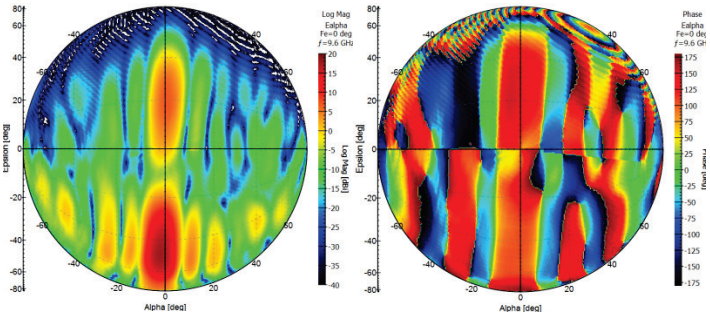

Figure 4. F-SAR X-band antenna on the bottom plate of the antenna carrier, left side: HH magnitude plots, right side: corrected phase plots

B. *Benefit of this method*

The electrical distance of the antennas' phase center in xyz-direction to the rotational origin of the measurement system can be precisely estimated from the phase history of the acquired antenna data. Measurement results show that antennas have individual phase centers for H- and V-polarization that may be in front or behind the surface of the aperture and vary with frequency. Figure 5 illustrates the traces of the phase center analysis of the two polarimetric F-SAR X-band antennas, mounted on the upper and on the lower left region of the antenna carrier.

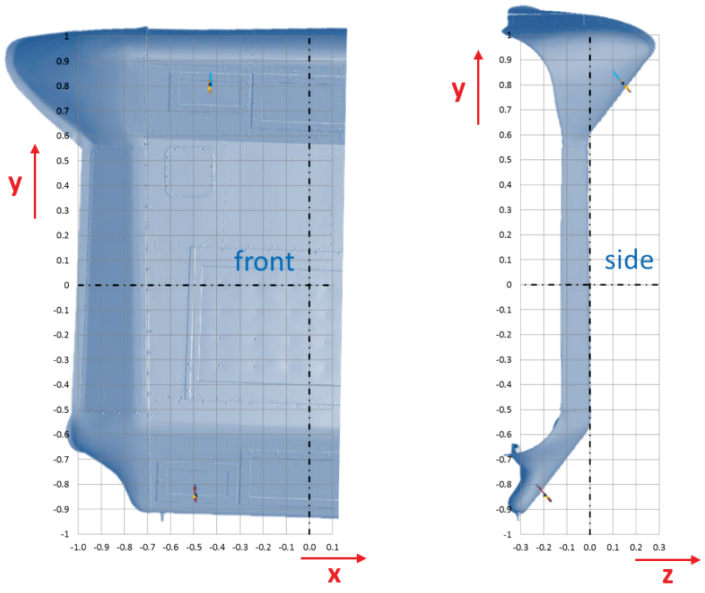

Figure 5. HH/VV phase center variation over the measurement bandwidth of the F-SAR X-band antennas

Motion compensation in the SAR processor asks for the lever arm of the Inertial Measurement Unit (IMU) on the airborne platform to each antenna phase center for precisely correcting the variations on the flight path. As well, the image focusing is based on the exact knowledge of the phase center.

Moreover, there is a significant influence of the carrier structure to the pattern, depending on the antenna position and the polarization. Figure 6 shows the projection of a far field to near field transformation of two identical X-band antennas at different mounting positions on the antenna carrier. Especially, the pattern of the upper X-band antenna (see figure 3) suffers from the non-ideal position. The slanted mounting plate supports the electrical beam steering of the antenna, but the

long structure on the side of the cabin strongly interacts and adversely impacts the far field magnitude and phase diagrams of the antenna. That especially effects interferometric SAR acquisitions using both of the antennas.

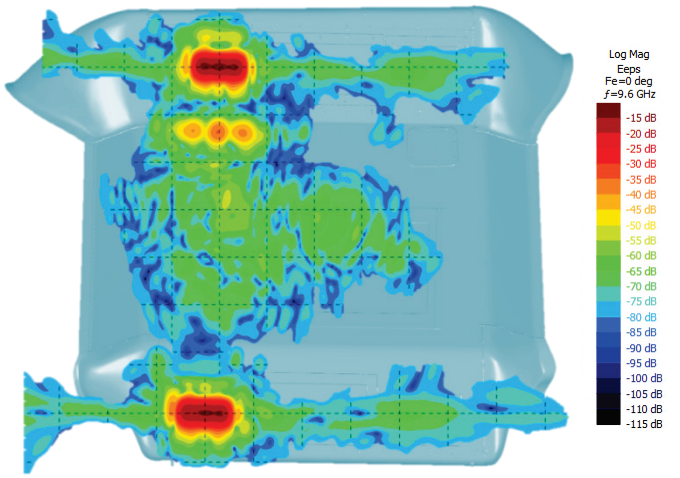

Figure 6. Far field to near field transformation of the F-SAR X-band antennas (VV) in boresight projection on the antenna carrier.

It should be noted that the far-field to near-field transformation is limited in resolution to $\lambda/2$. Only the radiating modes of the antenna can be measured in a far-field acquisition. There, the evanescent near-filed modes are not present and cannot be retrieved using a far-field to near-field transformation. Higher resolutions may only be achieved by capturing both, the radiating and the evanescent modes of the antenna.

III. Use of the Antenna Patterns in F-SAR Image Processing

A. Radiometric calibration

The radiometric calibration, as shown in [4], is a tool in SAR processing to link the intensity in the focused SAR image to the radar cross section of a dedicated target on the site. Moreover, systematic brightness variations that result from the non-isotropic antenna patterns and the flying platform attitude must be removed. The complex 3D theta-phi antenna patterns are measured for P-, L-, S-, C- and X-band. By coordinate transformation, elevation over azimuth and frequency antenna patterns are available for the co- and cross-polar transmit and receive path. The SAR sensor is illuminating the area perpendicular to the moving direction of the flying platform with an FM chirp transmit pulse. On the SAR receiver side, the backscattered signals simultaneously arrive over the complete FM frequency range. To take that into account, a 2D antenna gain is obtained in the F-SAR processor with integrating over the processed frequency range for a given transmit and receive combination.

A dedicated calibration test site is used for the analysis of the F-SAR sensor system performance prior to flight campaigns. Figure 7 compares the newly implemented radiometric calibration technique that is using the 2D antenna gain over a system bandwidth of 300 MHz (bottom) in S- and in X-band for SAR processing with one used in the past that is simply using the antenna elevation pattern at the center frequency (top).

It is shown that the RCS error in both, S- and X-band, can be reduced significantly over a wide angular range. With applying the full 3D antenna patterns, the RCS standard deviation was reduced from 0.36 dB to 0.26 dB.

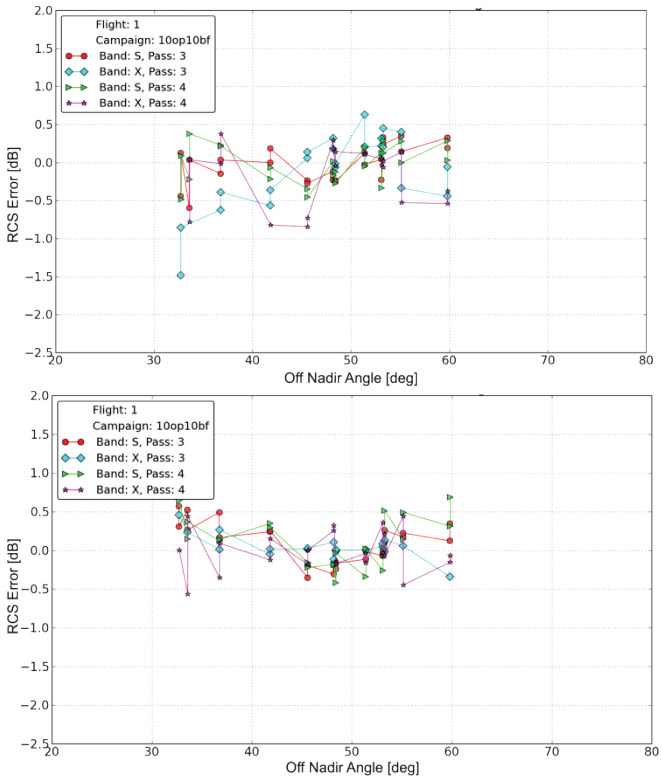

Figure 7. RCS error of the measured trihydral corner reflectors with respect to their theoretical values. The plots show F-SAR acquisitions in S-band and in X-band with a 300 MHz system bandwith Top: Based on a 1D elevation pattern of the antenna; Bottom: Based on the 2D antenna patterns that are integrated over the bandwidth.

B. Polarimetric calibration

Polarimetric SAR acquisitions comprise multiple channels with different transmit and receive polarizations acquired simultaneously. In addition to radiometric accuracy, polarimetric calibration also requires that the inter-channel phase differences be calibrated. To improve the phase calibration, the phase information in the 3D antenna pattern is exploited in a fashion similar to the one adopted for radiometric calibration. From the 3D antenna pattern, a phase map at the center frequency is extracted.

A phase correction for a given resolution cell is then obtained by integrating, for each resolution cell in an acquisition and taking into account sensor attitude angles, the antenna phase contribution over the illumination time. A more detailed description is given in [1].

Figure 8 demonstrates the improvement in the polarimetric calibration that is achieved by applying the antenna phase correction in the processing.

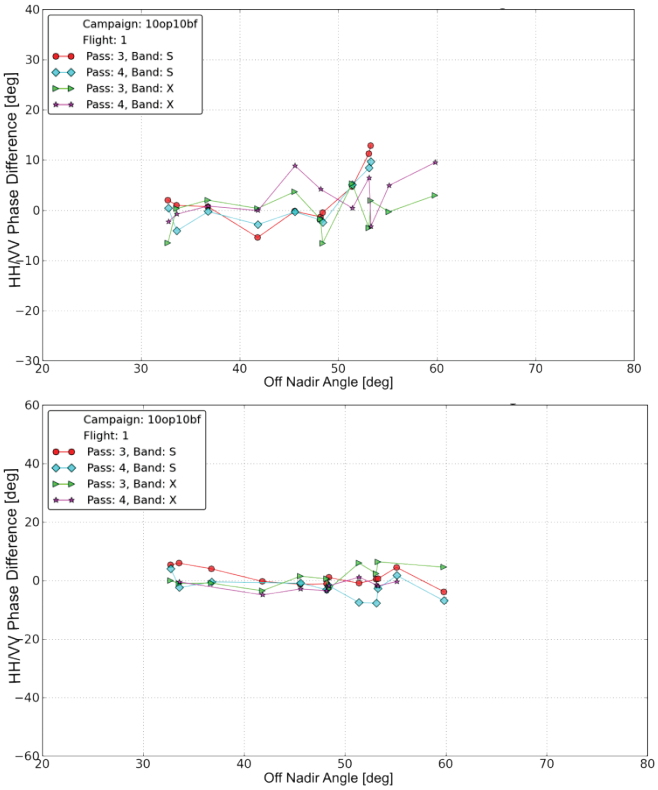

Figure 8. The phase difference between the HH and VV polarized channels measured on trihedral corner reflectors that is theoretically zero. HH/VV phase difference - Top: Without phase correction; Bottom: After phase correction

C. *Interferometry*

Much the same effects are seen in SAR interferometry; where the phase difference between two independent SAR acquisitions is measured to, for example, derive digital elevation models. If the two acquisitions are acquired with different antennas, as in the example of figure 9, the differential antenna phase becomes overlaid on the actual interferometric phase measurement.

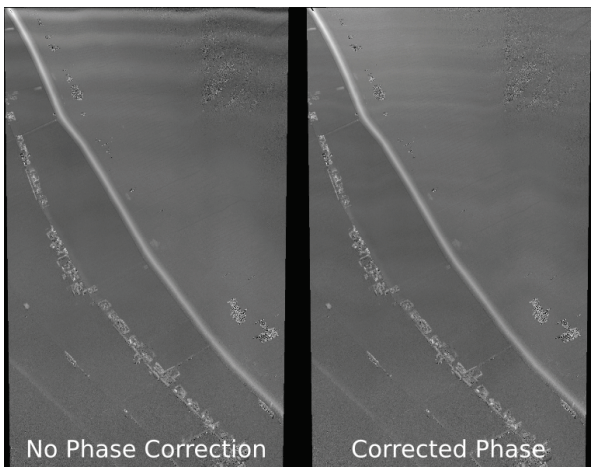

Figure 9. The interferometric phase measured by the F-SAR single pass across track interferometer at X-band. Left side: Without antenna phase correction with visible artefacts in the top half of the measurements. Right side: After the correction.

In the example shown, the antenna phase correction during processing largely suppresses the artifacts that otherwise arise due to interactions between the antennas and the carrier.

D. *Image Formation*

For accurately focusing the SAR image, the knowledge of the propagation characteristics in the antenna and its beam forming network is of high importance. The antenna measurements are typically calibrated with standard gain horns that interface to the Compact Test Range at a reference connector plane. The propagation delay in the antenna under test is then referenced to this calibration plane by the antenna analysis software.

IV. CONCLUSION

The results presented underline the importance of highly accurate, complex 3D antenna characterization in the processing and calibration of broadband SAR data. The antenna raw data is post processed and analyzed with a commercial but highly flexible engineering software tool [5]; the antenna parameters are extracted and interfaced to the F-SAR processor of the Microwaves and Radar Institute. Experiments using real SAR data have confirmed that compensating for propagation effects in the antenna affects all areas of SAR image quality: the radiometric calibration, the calibration of inter-channel phase differences in SAR polarimetry and, finally, the quality of interferometric phase measurements.

ACKNOWLEDGMENT

The author thanks L.G.T. van de Coevering from March Microwave Systems B.V. for continuously implementing new functionality to the antenna analysis tool ARCS 3.5.

REFERENCES

[1] M. Jäger, A. Reigber, R. Scheiber, “Accurate consideration of Sensor Parameters in the Calibration and Focusing of F-SAR Data,” Proceedings of the European Conference on Synthetic Aperture Radar 2012 (EUSAR 2012), pp. 20-23. VDE Verlag GmbH, Aachen Germany.

[2] A.C. Ludwig, “The Definition of Cross Polarization,” IEEE Trans. on Antennas and Propagation, Vol. AP-21 no 1, Jan. 1973, pp. 116-119.

[3] J. E. Roy, L. Shafai, “Generalization of the Ludwig-3 Definition for Linear Copolarization and Cross Polarization,” IEEE Trans. on Antennas and Propagation, Vol.. 49, No. 6, June 2001, pp. 1006-1020.

[4] A. Freeman, “SAR Calibration: a Review,” IEEE Trans. Geosci. Remote Sensing, Vol. 30, Nov. 1992, pp. 1107-1121.

[5] March Microwave Systems B.V., “ARCS Antenna and Radar Cross Section Measurement System Version 3.5 Analysis – Processing Reference Manual v1.38”, Nov. 2013.